Kelvin probe force microscopy under variable illumination: a novel technique to unveil charge carrier dynamics in GaN

Palmerina Gonzalez Izquierdo, Névine Rochat, Matthew Charles, Tomasz Sochacki, Lukasz Borowik

Kelvin Probe Force Microscopy under variable illumination: a novel technique to unveil charge carrier dynamics in GaN

Palmerina González-Izquierdo[1], Névine Rochat[1], Matthew Charles[1], Tomasz Sochacki[2] and Łukasz Borowik[1]**

[1]Univ. Grenoble Alpes, CEA, Leti, F-38000 Grenoble, France.

[2]Institute of High Pressure Physics, Polish Academy of Sciences, Sokolowska 29/37, 01-142 Warsaw, Poland

KEYWORDS: GaN, Gallium Nitride, III-V, Kelvin Probe Force Microscopy, Surface photovoltage, charge trapping, carrier dynamics, defects, dislocations, surface states.

ABSTRACT: GaN is a widely used material for optical and power devices. However, the performance of GaN-based devices is often reduced by charge trapping processes due to defect levels in the band gap. In this paper, we studied a GaN on silicon sample via Kelvin probe force microscopy (KPFM) under variable illumination. This novel methodology allows the surface photovoltage (SPV) to be followed on the GaN surface as a function of time, light intensity and topography with nanometric resolution. The measured SPV decay after turning off the light is too slow (on the order of seconds to days) to correspond to electron-hole recombination, suggesting that it is due to charge trapping. Two processes of opposite sign contributing to the SPV generation and decay were observed, indicating two different charge trapping mechanisms. In this study, we propose a model that accounts for the observed SPV behavior at different measurement temperatures. Furthermore, the contribution to the electronic behavior of possible contamination surface states is discussed.

Introduction:

Since the development of the blue LED in 1988,(1) GaN-based white LEDs have become the most efficient artificial light source,(2) being widely marketed and entering in most of our homes. Additionally, GaN-based mini- and micro-LEDs are strong candidates to replace the current liquid crystal displays (LCD) and OLED display technology.(3–5) Moreover, over the last decade, GaN materials and, particularly, GaN on silicon, is envisaged to gradually displace silicon in power devices due to its advantages with respect to Si, such as higher operating temperatures, higher breakdown field and higher switching speed.(6–8) However, there are still efficiency drawbacks that need to be solved. One of the main issues responsible for reducing the performance of GaN-based devices are defects, which are generated by a loss of the periodicity of the crystal lattice, either due to incorporation of foreign atoms (impurities) into the crystal or to a non-ideal arrangement of the host atoms during the growth of the material (native defects). The local perturbation of the periodic potential of the lattice introduces allowed energy states within the forbidden bandgap of GaN. In particular, one type of native defects is known to affect GaN-based devices efficiency: threading dislocations (TDs). These extended defects are generated due to the lattice mismatch between the GaN and the substrate (generally Si, SiC or sapphire) and propagate following the growth direction, producing pits on the GaN surface from a few to hundreds of nanometers, depending on the epitaxy structure.

In this work, we used Kelvin probe force microscopy or KPFM (one of the most sensitive methods to probe surface potential related to work function, with a sensitivity <5 meV) under variable illumination in order to study the charge carrier dynamics and charge trapping in a sample of GaN on Si near the surface. KPFM measures the contact potential difference (CPD) between a probing tip and the sample with nanometric resolution,(9) which makes it particularly suited for investigating dislocations. By measuring the CPD in darkness and under illumination, we can map the surface photovoltage (SPV), defined as the change in the surface potential induced by the reorganization of the photo-generated carriers. The SPV, therefore, can shed light onto the different processes of charge transport, recombination and trapping. Although KPFM under illumination is a well-established method to measure surface photovoltage and charge carrier lifetime in organic and inorganic materials,(10–14) the novelty of our approach consists in measuring the SPV while increasing the light intensity. This measurement method allows us not

only to observe the SPV decay once the light is turned off, but also to follow the SPV generation as a function of the laser power. Furthermore, KPFM is performed simultaneously with atomic force microscopy (AFM), allowing for the correlation of the spatial distribution of CPD and SPV with the surface's topography and, therefore, the dislocation pits.

Experimental methods:

The studied sample consists on as-grown unintentionally doped wurtzite GaN (1700 nm) on a Si(111) substrate doped with boron (1 mm) by metal-organic vapor phase epitaxy (MOVPE). The buffer layers are, from top to bottom: GaN:C (400 nm), AlGaN (24% Al, 900 nm), AlGaN (36% Al, 400 nm) and AlN (400 nm). A dislocation density of approximately $9x10^8$ cm^{-2} was estimated by cathodoluminescence at room temperature (RT) using an Attolight CL microscope (primary electron beam energy 3 keV, beam current 3 nA). The sample was stored in air for several months prior to this study.

Free-standing undoped and Si doped GaN samples, for comparative complementary measurements, were crystalized from the gas phase by halide vapor phase epitaxy (HVPE) on ammonothermally grown GaN seed.(15–17) HVPE-GaN crystals obtained in this way are with high structural quality in the terms of high radii of crystallographic planes, which exceeds 20 m, narrow X-Ray diffraction rocking curves and low threading dislocation density ($5{\cdot}10^4$ cm^{-2}, estimated by etching in molten KOH–NaOH eutectic). (18,19)

The sample surface chemical analysis was performed with a VersaProbe II spectrometer from Physical Electronics using a high-resolution monochromatic Al Kα line X-ray source at 1486.6 eV. The photoelectron takeoff angle was 45°, which provided an integrated sampling depth of approximately 5 nm. XPS data was collected at room temperature, after heating in vacuum for 1 h at 220° C and after soft (0.5 kV, 1 μA) Ar+ sputtering in a 2x2 mm2 area for 2 min, in that order.

In this work, we used non-contact atomic force microscopy (nc-AFM) using a VT-AFM from Scienta Omicron, interfaced with a Nanonis controller from SPECS Zürich, operating in ultra-high vacuum ($<10^{-10}$ Torr). We used a metal-plated conductive tip (EFM PPP, from

Nanosensors) with a resonant frequency f_0 between 45 and 115 kHz (nominal value 75 kHz). For nc-AFM, the tip was mechanically excited at f_0 with a feedback loop on the frequency shift to keep the distance between tip and sample constant (FM-AFM).

We performed heterodyne KPFM (h-KPFM) and AFM simultaneously during the experiments. Heterodyne KPFM combines the advantages of AM- and FM-KPFM by using an additional lock-in amplifier (HF2LI from Zurich Instruments).(20–22) In h-KPFM, a modulated bias voltage V_{ac} is applied with frequency $f_1–f_0$ (f_0 and f_1 are the fundamental resonant frequency and its first harmonic, respectively), which generates an electrostatic force at f_1 when the cantilever's bias V_{dc} does not match the contact potential difference. To measure V_{CPD}, a feedback loop is introduced to nullify the cantilever's oscillation amplitude at f_1. The potential sensitivity was enhanced with an increased quality factor due to the ultra-high vacuum (UHV) conditions, making h-KPFM under UHV well suited for surface potential measurements.(20) In order to generate surface photovoltage, we used an external fiber-coupled laser (PhoxXplus module from Omicron Laserage GmBH) at 405 nm through a viewport of the UHV chamber. Additionally, we measured the photon flux with a power meter (standard photodiode power sensor from Thorlabs). The sample was electrically grounded by the bottom (Si substrate) using a conductive biphasic silver epoxy.

The measurement protocol employed in this investigation consisted of dividing the sample's surface into a grid of pixels and measuring, simultaneously, the topography and the V_{CPD} as a function of the laser power (Figure 1.a). On each pixel, the laser is turned on and its power is increased linearly until arriving at a plateau of the $V_{CPD.}$ Then, the laser is switched off, and the measurement continues until the V_{CPD} comes back to the initial state in darkness. This method allowed us to follow the SPV during the generation/trapping and recombination/de-trapping of charges, giving us information about the charge carrier dynamics on the system rather than a static picture (see example of the SPV curve as a function of time and laser power in one pixel in Figure 1.b) and relate it to the surface's topography (see example of the SPV map at a specific time data point in Figure 1.c). During this experiment, there was a weak parasitic illumination at approximately 10 s during the measurement protocol, caused by the non-linear response of the laser at low applied bias (see Figure S1).

In order to further study the trapping mechanisms in our sample, we performed measurements at low temperature to partially freeze the defect states. We used liquid nitrogen (LN2) and liquid helium (LHe3) to cool the sample, by pumping the cooling fluid towards a secondary chamber in which there are Cu conducting cables connected to the sample holder. The temperature was measured by a thermocouple on the sample holder, registering 115 K for LN2 and 33 K for LHe3. It is highly probable that this temperature is slightly different on the sample's surface.

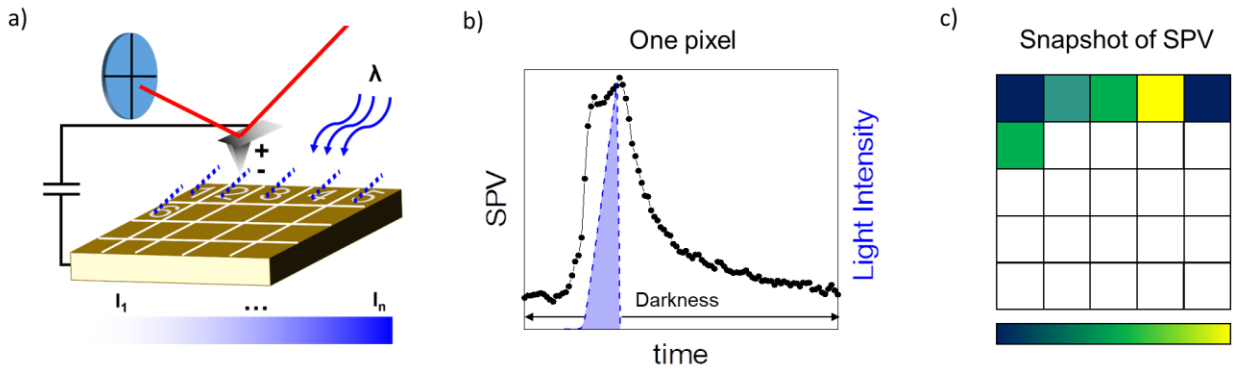

Figure 1. a) Schematic of KPFM under variable illumination measurements. b) SPV curve vs. time as a function of the laser power in one pixel. c) Map of SPV at a specific moment in time.

Results and discussion:

To perform the KPFM under variable illumination measurements, we first identified a small area (800 x 800 nm^2) with as many dislocations as possible. In this case, we focused on an area with three dislocations, as shown in the topographic map obtained through AFM in Figure 2.a. We divided this area in 64 by 64 pixels, in order to have enough resolution to see the dislocations, which are around 40 nm wide. Figure 2.b shows the CPD map in darkness, corresponding to the first data point of each pixel (t = 0 s). A larger, more resolved topography scan and its corresponding CPD map (2 x 2 μm^2, 512 x 512 px^2) are available in the SI in Fig. S3. By comparing the CPD map to the topography, we can see that dislocation pits are located in areas with higher CPD (between 150 and 200 mV difference) which, in our setup, means more positively charged regions. This finding differs from previous studies, which observed/predicted negatively

charged dislocations.(23–29) However, these negative fixed charges at dislocations are not seen in every sample: some studies measured no charge density on TDs (30,31) and other reported even positively charged dislocations.(32,33),(34) KPFM is sensitive to the surface states and, therefore, to any possible contamination layer (oxide, carbon complexes, adsorbed water, etc.) which, in turn, depends on the growth process, the cleaning process, if any, and the time and conditions of storage, making the comparison of samples difficult. In our case, the samples were stored in air for several months prior to the KPFM protocol. The XPS results (Figure S2) revealed the presence of O and C (relative atomic concentration respect to the Ga3d peak: 29.2% and 44.0%, respectively). The CPD values increase in certain areas but are not linked to dislocation pits in the AFM map (Figs. 2.b and S3). This could be because there are dislocations that do not end in large enough pits to be visible in the surface morphology scan, but they can still be observed using KPFM because the electrostatic forces have a longer range than the van der Waals forces. In Figure 2.b and S3, only screw or mixed type dislocations are visible, which are identified by their appearance at the termination of atomic steps. Therefore, it is probable that pure edge type dislocations have not been imaged by AFM for this particular sample. Inversely, although not displayed in Figure 2 (see Fig. S3), some dislocation pits do not show variation in CPD. These could be pure screw TDs, which are reported to be electrically inactive. (24,29,30)

Figures 2.c and 2.d show the CPD and SPV curves as a function of time and laser power at five different pixels, marked on the AFM and CPD maps. Pixels 1, 2 and 3 are placed on the center of the three dislocation pits, pixel 4 corresponds to an area far away from the dislocation pits and pixel 5 was chosen on a maximum of the CPD without being associated with a dislocation pit. Two processes with different signs contributing to the CPD/SPV are unveiled by the linear increase of laser power. First, there is a drop to negative values at around 12 s (corresponding to low power laser values due to the non-linear parasitic illumination, discussed in the experimental methods section above). When further increasing the laser power, there is an increase of SPV until reaching a maximum and then the tendency changes and the SPV decreases. When the light is turned off, the SPV briefly increases for about 2 s before starting to decay in an exponential manner. Pixel 4, far away from dislocations, shows the highest SPV during illumination (the SPV has less of a reduction by the first process at this position). Figure 2.e shows the SPV map at maximum laser power (12 mW, t = 29 s), which shows areas with lower SPV related to TDs (pits on the topography map and/or potential peaks on the CPD map). As the surface band bending of GaN is in

accumulation,(35) meaning that the holes should be attracted to the surface, the lowering of the SPV can be related to a lower band bending at dislocations, to the trapping of electrons at dislocations, or to a combination of both. It is worth noting that we are able to generate surface photovoltage even though we illuminate with sub-band gap energy (for GaN and the AlN and AlGaN buffer layers), which indicates that the photons generate electron-hole pairs from/to defect energy levels. This is consistent with the literature, in which photo-current was measured below band-gap excitation,(35–37) and with complementary measurements performed in high-quality freestanding GaN samples (sample details in experimental methods), which did not show SPV. Another possible origin of SPV could be charge carrier generation on the underlying epitaxial layers, as light absorption is very low below the band gap. However, the carrier generation would still occur through defect levels in the AlN and AlGaN buffer layers (laser energy lower than the band gap) and seems unlikely on Si, as almost no SPV signal was measured using a laser of 2.7 eV, much greater than the Si band gap (1.11 eV).

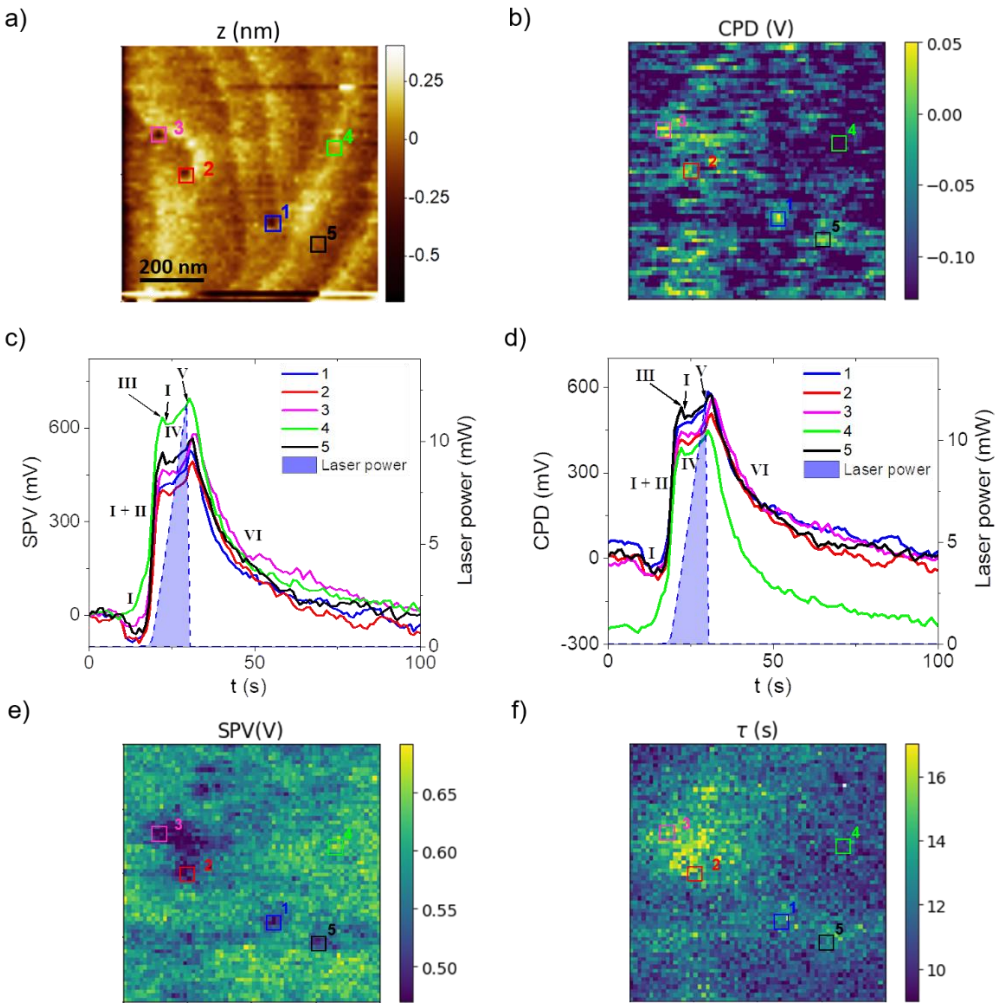

Figure 2. a) Topography of GaN on Si, 800 x 800 nm^2, 64 x 64 px^2 and b) CPD map in darkness (t = 0 s). c) CPD and d) SPV as a function of time and laser power at 5 different pixels of the surface, marked in the maps with different colors. Pixels 1, 2 and 3 are placed on the center of the three dislocation pits, pixel 4 corresponds to an area far away from the dislocation pits and pixel 5 was chosen on a maximum of the CPD without being associated with a dislocation pit. e) SPV at maximum laser power (12 mW, t = 29 s) and f) time decay constant maps.

Figure 2.f shows the time decay constant map resulting from fitting an exponential decay to the data observed after turning off the laser in each pixel. The decay, of the order of tens of seconds, is extremely long if we compare it with the reported carrier lifetimes for GaN, of the order of ns(38–41). However, the measured decay time is on the order of some traps' emission rate, such as a hole trap associated to carbon-related defects.(42) Analogously, very slow restoration of the

dark band bending reported by S. Sabuktagin *et al*.,(35) was attributed to charging and discharging of the surface states. This implies that the SPV does not come only from generation and recombination but also from trapping and de-trapping of charge carriers.[43]–[45] We can see in Figure 2.f that the time decay constant is greater in the areas related to dislocations, meaning higher trapping. In reality, this de-trapping process is even longer, of the order of days, confirmed by two separate measurements under variable illumination after keeping the sample for 3 and 10 days in darkness (see Figure S4).

We now propose a hypothesis for the charge carrier dynamics on GaN on Si during and after illumination in order to explain the observed SPV behavior. A simplified scheme for the different stages of the process is shown in Figure 3 (these steps are also marked in the CPD and SPV curves in Figures 2.c and 2.d, respectively). In our model, the surface photovoltage is caused by acceptor levels above E_c-0.72 eV, as laser energies below 2.71 eV induce little SPV. When turning on the laser with an energy of 3.06 eV, lower than the GaN band gap, electrons do not get enough energy to jump from the valence to the conduction band, but they do acquire enough energy to be promoted to the acceptor levels and become trapped (**I**). This process would be the origin of the SPV drop at low laser powers, which is highly probable at dislocations due to a high density of acceptor levels or the inactivation of these levels outside TDs due to surface states. This can be appreciated by comparing the CPD/SPV curves measured on dislocations and outside of dislocations, shown in Figures 2.c and 2.d. At the same time, due to the upward band bending, the photo-generated holes in the valence band accumulate at the surface, where they are captured by surface states (**II**).(35) This trapping of holes at the surface would be responsible for the SPV increase under illumination. As positive charge at the surface increases, the band bending decreases until all the surface states are filled with holes (**III**). With this model, we can explain the trend shift in SPV during illumination, occurring when this flattening of the surface band-bending takes place. In this way, the process responsible for the increase of SPV, i.e. accumulation and trapping of holes in the surface, stops, but the capture and trapping of photo-generated electrons by defect levels continues. In the same way, when the defect levels fill up (**IV**), the electron capture by these levels ceases, resulting in a plateau in SPV. When turning off the laser, the reverse processes take place, that is, the electrons de-trap from the defects (**V**), which increases the SPV, and the holes are slowly released from the surface states (**VI**), causing the SPV decay.

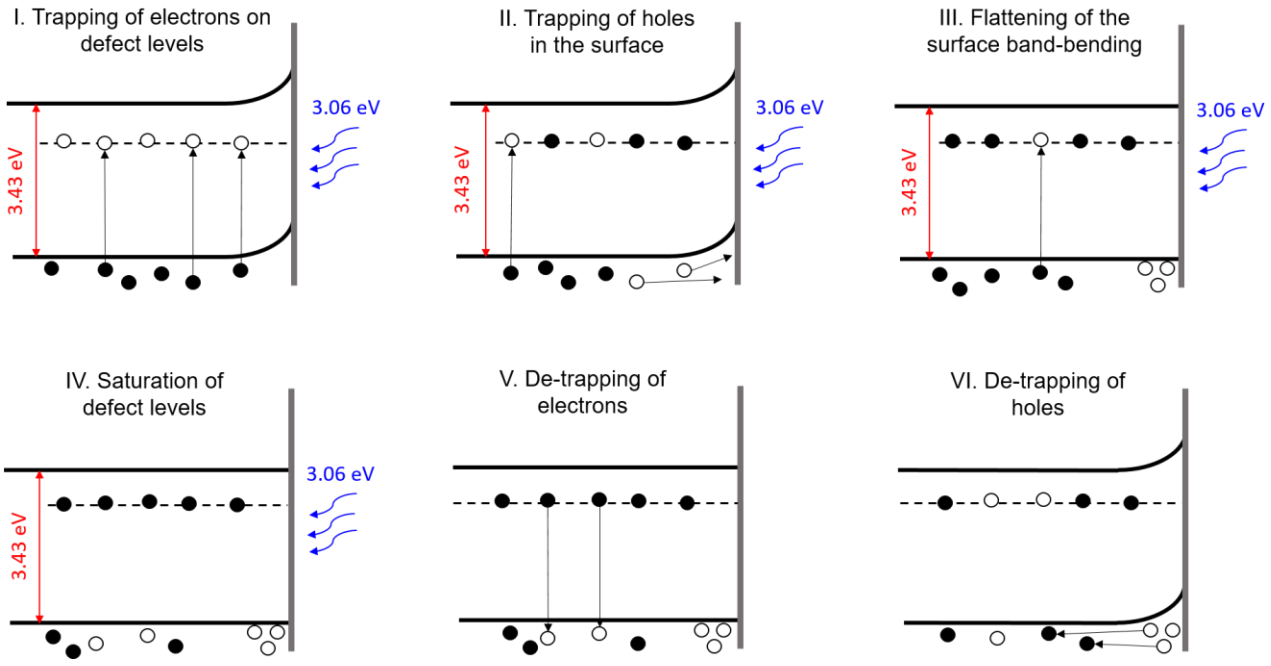

Figure 3. Scheme of the charge carrier dynamics during (**I-IV**) and after (**V-VI**) sub-band gap illumination.

Figure 4 shows the averaged SPV in a random area on the GaN surface at three different temperatures for three different maximum laser powers. As the measurements were done on GaN surface without prior dislocation localization, there is a much lower probability that the measurements are influenced by a high density of acceptor states linked to TDs. This lower probability of the influence of acceptor states can be confirmed by the measurement at RT (Figure 4a) where the process **I** is not visible for low laser power. However, it must be noticed that this process exists, as process **V** can be detected by the increase of SPV/CPD after the light extinction. We want to point out that, at RT, all types of de-trapping processes are happening simultaneously, even during illumination (together with the trapping processes). At low temperature, the de-trapping processes are less probable due to the freezing out of defects, meaning that the trapped charges need some thermal energy to be released. In this way, when decreasing the temperature, the defect energy levels are occupied (charges are trapped) and there is not enough energy to promote the charge carriers, thus preventing the electronic levels from emptying. As a

consequence, transitions through the energy levels introduced by defects are not possible, resulting in the suppression of the de-trapping channels. Due to the lower probability of de-trapping at low temperature, the SPV under illumination will be mainly influenced by the trapping processes. Consequently, the two trend shifts in SPV, corresponding to the two previously described trapping mechanisms (**I** and **II**), are more pronounced when lowering the temperature, as seen in Fig. 4. For the same reason, after the light extinction, the trends linked to charge de-trapping (**V** and **VI**) are also more pronounced, as more charges were accumulated under illumination, especially at 33K for process **V**, where the electrons from the defect levels de-trap for a longer time (Figure 4,c). While the SPV after turning off the light appears to follow a combination of exponential growth and decay at room temperature and 115 K, the same behavior is not observed at 33 K, where process **VI** appears to start once process **V** has concluded. This delay may be caused by electrostatic fields that link the two de-trapping processes and increases with decreasing temperature. However, given the complexity of the observed behavior, we cannot draw any firm conclusions from the data at hand. Finally, a minimum laser power is needed to trigger the SPV trend shifts, as seen in Figure 4 for the weakest power laser ramp for the three measured temperatures, in which the SPV shows a much simpler evolution: growing with increasing laser power and decaying immediately after turning off the light. This feature is consistent with our model, for which a minimum number of photons has to be reached in order to saturate the surface state levels (**III**).

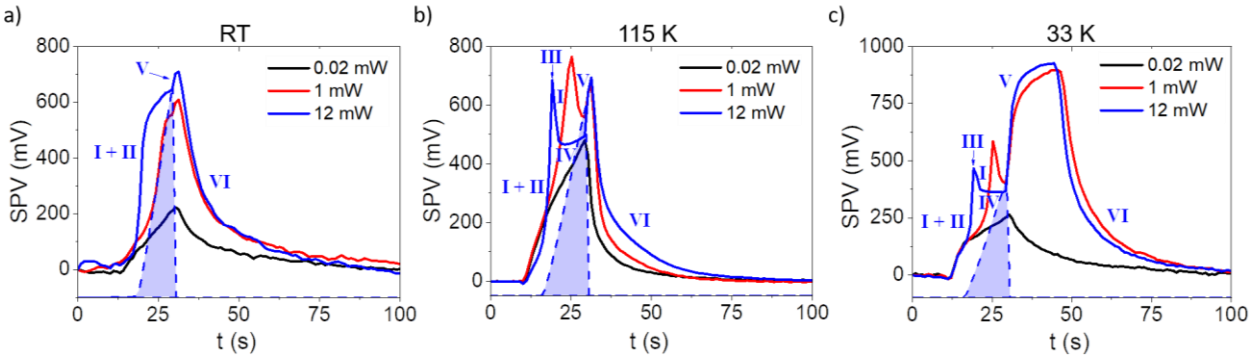

Figure 4. SPV vs. time at RT (mean over 4 x 4 µm^2, 3 x 3 px^2), 115 K (mean over 2 x 2 µm^2, 3 x 3 px^2) and 33 K (mean over 2 x 2 µm^2, 9 x 9 px^2) as a function of three different maximum laser powers: 12 mW (blue), 1 mW (red) and 0.02 mW (black). Only shown one power intensity ramp and its corresponding trapping/de-trapping processes for the sake of clarity.

Additionally, we submitted the sample to a surface treatment (heated at 220°C for 1 hour in UHV) in order to get rid of possible surface states, most likely adsorbed water.(31,46,47) The XPS measurements after heating (following the same heating procedure under standard vacuum) reveal a decrease in the O1s line, from 29.2% before heating to 25.8% after heating (Fig. S2.b), and an increase in the C1s line, from 44.0% before heating to 46.5% after heating (Fig. S2.c). Although the total percentage of carbon slightly increases, maybe due to degassing of the sample holder during heating, the C1s peak associated to oxygen bonding decreases (see Fig. S2.c). After soft Ar^+ sputtering, no presence of C or O is detected (Fig. S2), indicating that the contamination only comes from the surface. Figure 5 corresponds to an analogous measurement to that depicted in Figure 2 after heating the sample. In this case, two dislocations are clearly visible in the AFM map (Figure 5.a). Once more, not all the dislocation pits observed in the topography map are visible on the CPD map and vice versa (difference between edge, screw and mixed TDs), (24,29,30) only this time those showing a variation in CPD do it as a drop in potential (see Figure 5.b and S5). This lower value of CPD indicates that these extended defects are negatively charged, in agreement with the literature,(23–29) confirming the modification of the surface states. Another group reported that oxide formation occurs preferentially at dislocations,(48) so it is possible that other impurities, such as hydroxide groups or moisture, would also be found preferentially at TDs. However, the CPD and SPV curves show a similar overall behavior to that of the pre-heated sample, with the two contributions of different signs attributed to the trapping of electrons and holes described previously (different stages of the process marked in Figures 5.c and 5.d). Nonetheless, in this case, there is no correlation between the SPV and the position of dislocation pits, as seen in Figures 5.e and 5.f, corresponding to the SPV map at maximum laser power (12 mW, t = 29 s) and the time decay constant map. This finding indicates that process **I**, related to the trapping of electrons, happens everywhere in the sample and the involved acceptor levels are not related to TDs. Therefore, the lower SPV observed on dislocations on the sample before the thermal treatment must come from the surface states, most likely related to adsorbed water. These surface states either introduced new acceptor levels, reduced the band bending on TDs or deactivated the acceptor states outside dislocations, from which we can infer that TDs have influence on the aging of GaN.

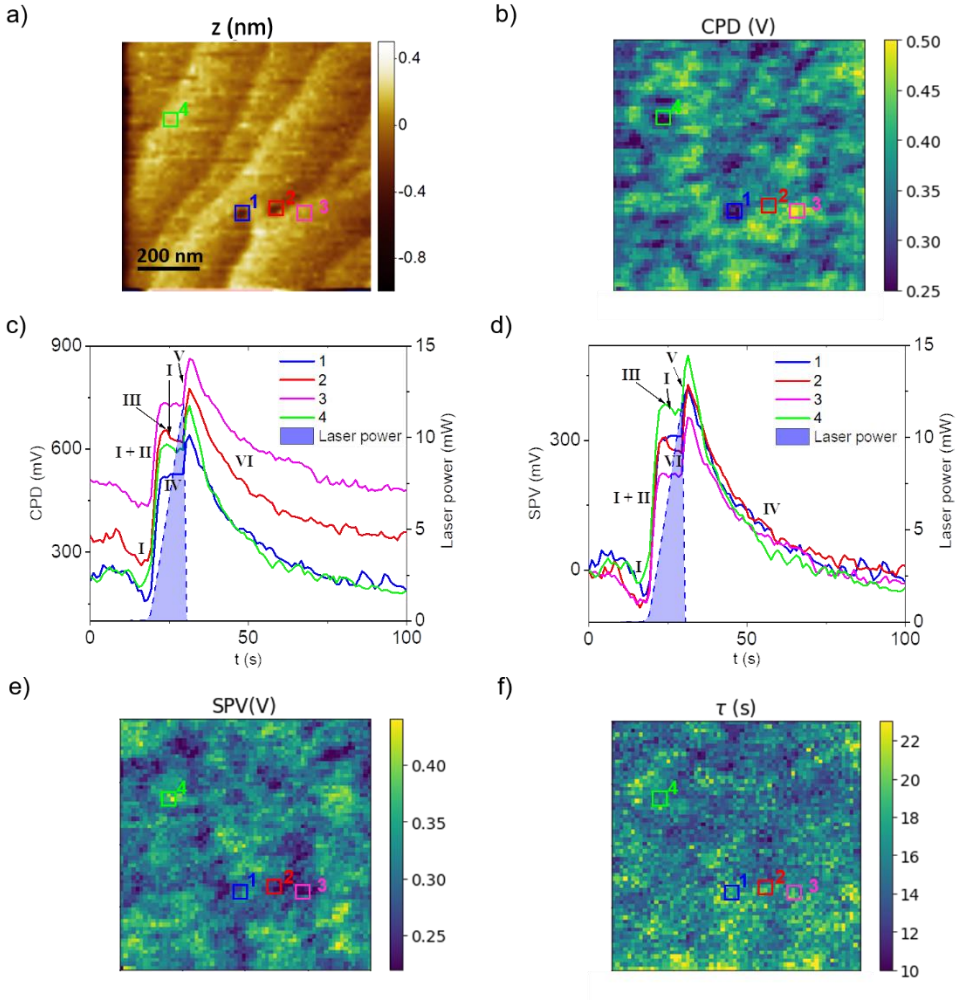

Figure 5. a) Topography of the GaN on Si sample after thermal treatment, 800 x 800 nm^2, 64 x 64 px^2 and b) CPD map in darkness (t = 0 s). c) CPD and d) SPV as a function of time and laser power at 5 different points of the surface, marked in the maps with different colors. e) SPV at maximum laser power (12 mW, t = 29 s) and f) time decay constant maps.

Conclusion:

In this work, we have used a novel technique based on KPFM under variable illumination on a sample of GaN on Si, which allowed us to follow not only the SPV decay after turning off the light but also the SPV generation as a function of the laser power. Moreover, the nanometric resolution

of this experimental technique makes it well suited for the study of dislocations, which produce pits on the surface of GaN of a few 10s of nanometers. Our results show very long SPV decay timescales, of the order of seconds to days, indicating the presence of trapping of charge carriers. Furthermore, two processes contributing to the SPV with different signs were observed, which we attributed to the trapping of electrons on shallow acceptor defect levels and to the trapping of holes in surface states due to the upwards band bending at the GaN surface. Although the observed signal could be due to deeply buried SPV on the interface between the epitaxial under-layers, the proposed charge transfer model may still be applicable to the buffer layers, as defects would still be responsible for generating the SPV (excitation energy lower than their band gaps).The proposed model is in agreement with additional measurements performed at low temperatures, with different trapping and de-trapping rates for the two processes. This model is also consistent with the SPV signal for different laser powers, a minimum number of photons being necessary to saturate the defect energy states. Finally, we submitted the GaN on Si sample to a thermal treatment in order to modify any possible surface states, most likely by water or hydroxide group desorption. Although the SPV tendency as a function of laser power was similar to the pre-heated sample, there was no correlation between the SPV variation and the position of dislocations, contrary to the previous results. This observation indicates that the SPV variation on dislocations observed before the thermal treatment originated from contamination surface states and, therefore, that TDs influence the aging of GaN.

ASSOCIATED CONTENT

Supporting Information (PDF). SPV curve in logarithmic scale; XPS results before heating, after heating and after sputtering; SPV after days in darkness; AFM and CPD maps (before and after heating) of larger areas with higher spatial resolution than the ones presented here.

AUTHOR INFORMATION

Corresponding Author

*Łukasz Borowik – Université de Grenoble Alpes, CEA, Leti, F38000 Grenoble, France

Email: lukasz.borowik@cea.fr

*Palmerina González Izquierdo – Université de Grenoble Alpes, CEA, Leti, F38000 Grenoble, France

Email: palmerina.gonzalezizquierdo@cea.fr

Author Contributions

P.G.I and Ł.B. measured and analyzed the KPFM under variable illumination data. N.R. measured and analyzed the cathodoluminescence data. M.C. grew the sample. T. S. grew high quality GaN. P.G.I. and Ł.B. conceptualized the project and wrote the paper, with input from all other authors. All authors have given approval to the final version of the manuscript.

Funding Sources

This work, performed on the Platform for NanoCharacterisation (PFNC) of CEA, was supported by the "Recherche Technologique de Base" Program of the French Ministry of Research and Carnot funding of the French National Research Agency (ANR), as well as was supported by PowerElec project, which has received funding from the EMPIR programme.

ACKNOWLEDGMENTS

This work, performed on the Platform for NanoCharacterisation (PFNC) of CEA, was supported by the "Recherche Technologique de Base" Program of the French Ministry of Research and Carnot funding of the French National Research Agency (ANR), as well as the EMPIR programme.

We also acknowledge the work of Julia Simon, Patrick Le Maitre and Marion Volpert, from CEA Leti, for their involvement in the fabrication of the sample.

REFERENCES

1. Akasaki I. High efficiency blue LED utilizing GaN film with AIN buffer layer by MOVPE. Inst Phys Coference Ser. 1988;91:633.
2. Cho J, Park JH, Kim JK, Schubert EF. White light-emitting diodes: History, progress, and future. Laser and Photonics Reviews. 2017. p. 1600147.
3. Templier F. GaN-based emissive microdisplays: A very promising technology for compact, ultra-high brightness display systems. J Soc Inf Disp. 2016;24(11):669–75.

4. Wang Z, Shan X, Cui X, Tian P. Characteristics and techniques of GaN-based micro-LEDs for application in next-generation display. Journal of Semiconductors. 2020. p. 041606.
5. Wasisto HS, Prades JD, Gülink J, Waag A. Beyond solid-state lighting: Miniaturization, hybrid integration, and applications of GaN nano-and micro-LEDs. Applied Physics Reviews. 2019. p. 041315.
6. Amano H, Baines Y, Beam E, Borga M, Bouchet T, Chalker PR, et al. The 2018 GaN power electronics roadmap. Journal of Physics D: Applied Physics. 2018. p. 163001.
7. Roccaforte F, Fiorenza P, Greco G, Lo Nigro R, Giannazzo F, Iucolano F, et al. Emerging trends in wide band gap semiconductors (SiC and GaN) technology for power devices. Microelectronic Engineering. 2018. p. 66–77.
8. Meneghini M, De Santi C, Abid I, Buffolo M, Cioni M, Khadar RA, et al. GaN-based power devices: Physics, reliability, and perspectives. Journal of Applied Physics. 2021. p. 181101.
9. Melitz W, Shen J, Kummel AC, Lee S. Kelvin probe force microscopy and its application. Surface Science Reports. 2011. p. 1–27.
10. Aubriet V, Courouble K, Gros-Jean M, Borowik Ł. Correlative analysis of embedded silicon interface passivation by Kelvin probe force microscopy and corona oxide characterization of semiconductor. Rev Sci Instrum. 2021;92(8):083905.
11. Aubriet V, Courouble K, Bardagot O, Demadrille R, Borowik Ł, Grévin B. Hidden surface photovoltages revealed by pump probe KPFM. Nanotechnology. 2022;33:225401.
12. Fernández Garrillo PA, Borowik Ł, Caffy F, Demadrille R, Grévin B. Photo-Carrier Multi-Dynamical Imaging at the Nanometer Scale in Organic and Inorganic Solar Cells. ACS Appl Mater Interfaces. 2016 Nov 16;8(45):31460–8.
13. Hoppe H, Glatzel T, Niggemann M, Hinsch A, Lux-Steiner MC, Sariciftci NS. Kelvin probe force microscopy study on conjugated polymer/fullerene bulk heterojunction organic solar cells. Nano Lett. 2005;5(2):269–74.
14. Tennyson EM, Garrett JL, Frantz JA, Myers JD, Bekele RY, Sanghera JS, et al. Nanoimaging of Open-Circuit Voltage in Photovoltaic Devices. Adv Energy Mater. 2015;5(23):1501142.
15. Sochacki T, Bryan Z, Amilusik M, Collazo R, Lucznik B, Weyher JL, et al. Preparation of free-standing gan substrates from thick gan layers crystallized by hydride vapor phase epitaxy on ammonothermally grown GaN seeds. Appl Phys Express. 2013;6:075504.

16. Iwinska M, Sochacki T, Amilusik M, Kempisty P, Lucznik B, Fijalkowski M, et al. Homoepitaxial growth of HVPE-GaN doped with Si. J Cryst Growth. 2016;456:97–96.
17. Kucharski R, Sochacki T, Lucznik B, Bockowski M. Growth of bulk GaN crystals. Journal of Applied Physics. 2020. p. 050902.
18. Kirste L, Danilewsky AN, Sochacki T, Köhler K, Zajac M, Kucharski R, et al. Synchrotron White-Beam X-Ray Topography Analysis of the Defect Structure of HVPE-GaN Substrates. ECS J Solid State Sci Technol. 2015;4(324).
19. Bockowski M, Iwinska M, Amilusik M, Fijalkowski M, Lucznik B, Sochacki T. Challenges and future perspectives in HVPE-GaN growth on ammonothermal GaN seeds. Semiconductor Science and Technology. 2016. p. 093002.
20. Sugawara Y, Kou L, Ma Z, Kamijo T, Naitoh Y, Jun Li Y. High potential sensitivity in heterodyne amplitude-modulation Kelvin probe force microscopy. Appl Phys Lett. 2012;100:223104.
21. Ma ZM, Kou L, Naitoh Y, Li YJ, Sugawara Y. The stray capacitance effect in Kelvin probe force microscopy using FM, AM and heterodyne AM modes. Nanotechnology. 2013;24(22):225701.
22. Garrett JL, Munday JN. Fast, high-resolution surface potential measurements in air with heterodyne Kelvin probe force microscopy. Nanotechnology. 2016;27:245705.
23. Koley G, Spencer MG. Scanning Kelvin probe microscopy characterization of dislocations in III-nitrides grown by metalorganic chemical vapor deposition. Appl Phys Lett. 2001;78:2873–2875.
24. Hansen PJ, Strausser YE, Erickson AN, Tarsa EJ, Kozodoy P, Brazel EG, et al. Scanning capacitance microscopy imaging of threading dislocations in GaN films grown on (0001) sapphire by metalorganic chemical vapor deposition. Appl Phys Lett. 1998 May 4;72(18):2247–9.
25. Cherns D, Jiao CG. Electron holography studies of the charge on dislocations in GaN. Phys Rev Lett. 2001;234(3):924–930.
26. Leung K, Wright AF, Stechel EB. Charge accumulation at a threading edge dislocation in gallium nitride. Appl Phys Lett. 1999;74:2495–2497.
27. Ng HM, Doppalapudi D, Moustakas TD, Weimann NG, Eastman LF. The role of dislocation scattering in n -type GaN films. Appl Phys Lett. 1998 Aug 10;73(6):821–3.

28. Look DC, Sizelove JR. Dislocation scattering in GaN. Phys Rev Lett. 1999;82:1237.
29. Simpkins BS, Yu ET, Waltereit P, Speck JS. Correlated scanning Kelvin probe and conductive atomic force microscopy studies of dislocations in gallium nitride. J Appl Phys. 2003;94:1448–1453.
30. Hsu JWP, Manfra MJ, Lang D V., Baldwin KW, Pfeiffer LN, Molnar RJ. Surface morphology and electronic properties of dislocations in AlGaN/GaN heterostructures. J Electron Mater. 2001;30:110–114.
31. Xie T, Kishimoto S, Mizutani T. Measurement of surface contact potential of AlGaN/GaN heterostructure and n-GaN by Kelvin probe force microscopy. In: Physica Status Solidi C: Conferences. 2003. p. 2372–5.
32. Im HJ, Ding Y, Pelz JP, Heying B, Speck JS. Characterization of individual threading dislocations in GaN using ballistic electron emission microscopy. Phys Rev Lett. 2001;87(10):106802.
33. Law JJM, Yu ET, Haskell BA, Fini PT, Nakamura S, Speck JS, et al. Characterization of nanoscale electronic structure in nonpolar GaN using scanning capacitance microscopy. J Appl Phys. 2008;103:014305.
34. Sahoo P, Oliveira DS, Cotta MA, Dhara S, Dash S, Tyagi AK, et al. Enhanced surface potential variation on nanoprotrusions of GaN microbelt as a probe for humidity sensing. J Phys Chem C. 2011;115(13):5863–5867.
35. Sabuktagin S, Reshchikov MA, Johnstone DK, Morkoç H. Band bending near the surface in GaN as detected by a charge sensitive probe. In: Materials Research Society Symposium - Proceedings. 2003. p. 542–547.
36. Monroy E, Calle F, Muñoz E, Omnès F, Beaumont B, Gibart P. Visible-blindness in photoconductive and photovoltaic AlGaN ultraviolet detectors. J Electron Mater. 1999;28:240–245.
37. Muñoz E, Monroy E, Pau JL, Calle F, Omnès F, Gibart P. III nitrides and UV detection. J Phys Condens Matter. 2001;13(32):7115.
38. Dalapati P, Manik NB, Basu AN. Influence of temperature on different optoelectronic characteristics of InGaN light emitting diodes. Opt Quantum Electron. 2017;49(265).
39. Reklaitis I, Kudžma R, Miasojedovas S, Vitta P, Žukauskas A, Tomašiūnas R, et al. Photoluminescence Decay Dynamics in Blue and Green InGaN LED Structures Revealed

by the Frequency-Domain Technique. J Electron Mater. 2016;45:3290–3299.

40. Al Muyeed SA, Sun W, Peart MR, Lentz RM, Wei X, Borovac D, et al. Recombination rates in green-yellow InGaN-based multiple quantum wells with AlGaN interlayers. J Appl Phys. 2019;126:213106.
41. Meyer J, Liu R, Schaller RD, Lee HP, Bayram C. Systematic study of shockley-read-hall and radiative recombination in GaN on Al2O3, freestanding GaN, and GaN on Si. JPhys Photonics. 2020;2:035003.
42. Tokuda Y. (Invited) DLTS Studies of Defects in n-GaN. ECS Trans. 2016;75(4):39–49.
43. Chakraborty A, Ghosh S, Mukhopadhyay P, Das S, Bag A, Biswas D. Effect of trapped charge in AlGaN/GaN and AlGaN/InGaN/GaN heterostructure by temperature dependent threshold voltage analysis. Superlattices Microstruct. 2018;113:147–52.
44. Jung E, Jeong S, Ryou JH, Kim H. Deep-trap states of GaN-based light emitting diodes analyzed by space charge limited conduction model. J Nanosci Nanotechnol. 2017;17(10):7339–43.
45. Polyakov AY, Lee IH. Deep traps in GaN-based structures as affecting the performance of GaN devices. Materials Science and Engineering R: Reports. 2015. p. 1–56.
46. Diale M, Auret FD, Van Der Berg NG, Odendaal RQ, Roos WD. Analysis of GaN cleaning procedures. Appl Surf Sci. 2005;246(1–3):279–89.
47. Smith LL, King SW, Nemanich RJ, Davis RF. Cleaning of GaN surfaces. J Electron Mater. 1996;25:805–810.
48. Yamada T, Ito J, Asahara R, Watanabe K, Nozaki M, Nakazawa S, et al. Comprehensive study on initial thermal oxidation of GaN(0001) surface and subsequent oxide growth in dry oxygen ambient. J Appl Phys. 2017;121:035303.

TOC Graphic: